Journal of Applied Physics

Deactivation of silicon surface states by Al-induced acceptor states from Al–O monolayers in SiO_2

Cite as: J. Appl. Phys. **125**, 015301 (2019); https://doi.org/10.1063/1.5054703
Submitted: 02 September 2018 . Accepted: 13 December 2018 . Published Online: 04 January 2019

Daniel Hiller, Paul M. Jordan, Kaining Ding, Manuel Pomaska, Thomas Mikolajick, and Dirk König

View Online Export Citation CrossMark

ARTICLES YOU MAY BE INTERESTED IN

Perspective: Nanoscopy of charge kinetics via terahertz fluctuation
Journal of Applied Physics **125**, 010901 (2019); https://doi.org/10.1063/1.5079534

Phonon properties and thermal conductivity from first principles, lattice dynamics, and the Boltzmann transport equation
Journal of Applied Physics **125**, 011101 (2019); https://doi.org/10.1063/1.5064602

Realization of rhombohedral, mixed, and tetragonal like phases of $BiFeO_3$ and ferroelectric domain engineering using a strain tuning layer on $LaAlO_3$(001) substrate
Journal of Applied Physics **125**, 012501 (2019); https://doi.org/10.1063/1.5054372

Ultra High Performance SDD Detectors

AMETEK MATERIALS ANALYSIS DIVISION

See all our XRF Solutions

© 2018 Author(s).

Journal of Applied Physics ARTICLE scitation.org/journal/jap

Deactivation of silicon surface states by Al-induced acceptor states from Al–O monolayers in SiO_2

Cite as: J. Appl. Phys. **125**, 015301 (2019); doi: 10.1063/1.5054703
Submitted: 2 September 2018 · Accepted: 13 December 2018 ·
Published Online: 4 January 2019

View Online Export Citation CrossMark

Daniel Hiller,[1,a)] Paul M. Jordan,[2,b)] Kaining Ding,[3] Manuel Pomaska,[3] Thomas Mikolajick,[2,4] and Dirk König[5,a)]

AFFILIATIONS

[1]Research School of Engineering, Australian National University, Canberra, Australian Capital Territory 2601, Australia
[2]Nanoelectronic Materials Laboratory gGmbH (NaMLab), 01187 Dresden, Germany
[3]IEK5-Photovoltaik, Forschungszentrum Jülich, 52425 Jülich, Germany
[4]Institut für Halbleiter- und Mikrosystemtechnik, TU Dresden, 01062 Dresden, Germany
[5]Integrated Materials Design Centre, University of New South Wales, Sydney, New South Wales 2052, Australia

[a)]Authors to whom correspondence should be addressed: daniel.hiller@anu.edu.au and solidstatedirk@gmail.com

[b)]Present address: Melexis Dresden GmbH, 01109 Dresden, Germany.

ABSTRACT

Al–O monolayers embedded in ultrathin SiO_2 were shown previously to contain Al-induced acceptor states, which capture electrons from adjacent silicon wafers and generate a negative fixed charge that enables efficient Si-surface passivation. Here, we show that this surface passivation is just in part attributed to field-effect passivation, since the electrically active interface trap density D_{it} itself at the Si/SiO_2 interface is reduced by the presence of the acceptor states. For sufficiently thin tunnel-SiO_2 films between the Si-surface and the Al–O monolayers, D_{it} is reduced by more than one order of magnitude. This is attributed to an interface defect *deactivation* mechanism that involves the discharge of the singly-occupied dangling bonds (P_{b0} defects) into the acceptor states, so that Shockley-Read-Hall-recombination is drastically reduced. We demonstrate that the combined electronic and field-effect passivation allows for minority carrier lifetimes in excess of 1 ms on n-type Si and that additional H_2-passivation is not able to improve that lifetime significantly.

Published under license by AIP Publishing. https://doi.org/10.1063/1.5054703

I. INTRODUCTION

State of the art PERC (passivated emitter rear contact) solar cells[1] typically use a backside passivation that is optimized to contain a high density of fixed charges (Q_{fix}) together with a very low interface trap density (D_{it}).[2] However, in the PERC concept, a contact through the passivation is required, leading to a significantly increased carrier recombination below the contacts as well as additional processing steps. In contrast, passivating carrier-selective contacts on Si heterojunction solar cells allow for nearly recombination-free interfaces and extraction of either electron or holes and avoid local destruction of the passivation layers. These contacts can be based on thin intrinsic and doped hydrogenated amorphous Si or on dopant-free dielectric materials.[3] Examples for the latter include for electron selective contacts TiO_2,[4] tunnel-SiO_2/TiO_2,[5,6] LiF_x,[7] or MgF_2[8] and for hole selective contacts MoO_x[7,9,10] or WO_x.[10] However, temperature stability of these materials remains an issue[3,5,10] as well as the scalability and costs incurred with thermal evaporation under high vacuum when alternative standard methods such as sputter deposition or atomic layer deposition (ALD) cannot be used.

Recently, we demonstrated that one Al–O monolayer (ML) from a single ALD-Al_2O_3 cycle embedded in thin SiO_2 can create significant negative Q_{fix} and this enables efficient field-effect passivation combined with improved hole tunneling.[11] The origin of Q_{fix} was identified as Al-induced acceptor states at the SiO_2/Al_2O_3 interface with an energy level 0.5–0.8 eV below the Si valence band edge that capture

Published under license by AIP Publishing.

electrons from the Si substrate and that act as hopping sites for holes.[11,12]

In this contribution, the correlation between negative Q_{fix} and minority carrier lifetimes (τ_{eff}) as a function of the tunnel-SiO_2 thickness and the role of H_2-passivation are investigated. We show that the interface trap density at the Si/SiO_2 interface depends decisively on the thickness of the tunnel-SiO_2 between the wafer and the ALD Al–O MLs. A passivation mechanism is revealed in theory and experiment that involves the electronic deactivation of dangling bonds (DBs) at the Si/SiO_2 interface by interaction with the Al-induced acceptor states.

II. EXPERIMENTAL DETAILS

For lifetime measurements of double-side polished *n*-type, <100>-oriented Cz-Si wafers (~5 Ω cm, 525 μm thick) and for electrical characterization single-side polished *n*-type, <100>-oriented Cz-Si wafers (~2 Ω cm, 525 μm thick) were used. After RCA-cleaning (Radio Corporation of America) including a final HF-dip, a wedge-shaped tunnel-SiO_2 thickness gradient was fabricated by rapid thermal oxidation (RTO; 13 nm) and motorized dipping in diluted buffered HF (slant-etching) with an etch rate adjusted to fully etch the SiO_2 at the lower part of the wafer, followed by immediate rinsing in DI-water and subsequent deposition of 6 plasma-ALD Al_2O_3 cycles (~7.5 Å) and 20 nm capping SiO_2 (PECVD). Reference samples were identically processed except for omitting the trimethylaluminum (TMA) pulses during ALD, so that no Al–O MLs are grown. All samples were rapid thermally annealed (RTA) in pure Ar at 900 °C for 30 s to form the Al-induced acceptor states.[11] H_2-passivation took place in the pure-H_2 atmosphere for 1 h at 400 °C. Aluminum contacts for electrical characterization were thermally evaporated. High-frequency capacitance-voltage (C-V) and conductance-voltage (G-V) curves were measured at 300 kHz and interface trap densities were determined via the method proposed by Brews.[13] The interface state energy distribution over the bandgap was determined by quasi-static C-V measurements.[14] Effective minority carrier lifetimes were measured by microwave detected photoconductance (MDPmap, Freiberg Instruments GmbH) using a 976 nm laser with a power of 20 mW.

III. RESULTS AND DISCUSSION

Figure 1(a) shows the relative fixed charged densities ($Q_{fix,rel}$; derived from the flatband voltage (V_{FB}) shift[15] of the Al–O-samples (samples W) with respect to V_{FB} of the Al–O-free references (samples R), whose positive Q_{fix} are in the lower 10^{11} cm^{-2} range) as a function of tunnel-SiO_2 thickness. As demonstrated before, maximum $|Q_{fix}|$ values are observed in the range of ~2 nm tunnel-SiO_2.[12] Thicker tunnel-SiO_2 layers result in very low electron tunneling current densities from the substrate into the Al-induced acceptor states. In contrast to Ref. 12 (where thermal ALD was used for Al_2O_3 deposition), a clear minimum tunnel-SiO_2 thickness is hardly observed here. Hence, in the case of plasma-ALD for Al–O ML deposition, insufficient formation of

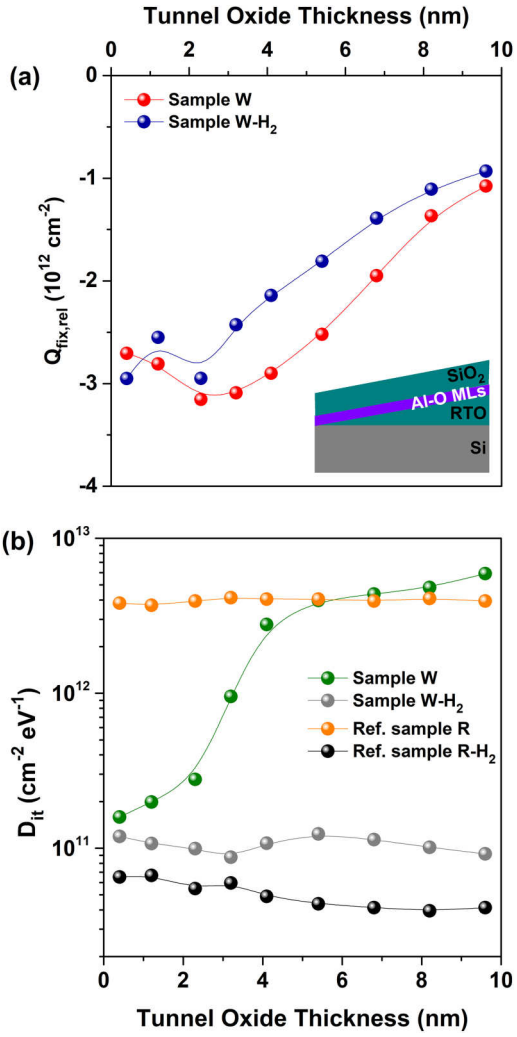

FIG. 1. (a) Relative fixed charge densities ($Q_{fix,rel}$) and (b) interface trap densities (D_{it}) of the samples with slant-etched, wedge-shaped tunnel-SiO_2 and 6 Al–O MLs before and after H_2-passivation, as a function of tunnel-SiO_2 thickness. The inset in (a) depicts a schematic cross section of the layer stack of sample W. All lines (splines) are just a guide to the eye. H_2-passivation causes a decrease in Q_{fix}. For ultra-thin tunnel-SiO_2 thicknesses, D_{it} is decreased to the level of H_2-passivated samples due to the discharge of DBs into Al-induced acceptor states in SiO_2.

acceptor states due to too thin (or fully etched) SiO_2 is less expressed due to the oxidation of the exposed Si-surface by the O-plasma.

The effect of H_2-passivation appears to be detrimental to the Q_{fix} density. Though there is little effect of H_2 on Q_{fix} for up to ~2.5 nm tunnel-SiO_2, the reduction is up to ~30% for thicker oxides (equivalent to a negative Q_{fix} loss of up to 7.5×10^{11} cm^{-2}). Taking the atomic structure of the Al-induced acceptor state in SiO_2 into account (i.e., a fully O-coordinated,

Published under license by AIP Publishing.

trivalent Al-atom replacing a Si-atom in the Si–O tetrahedrons of SiO_2, which creates an O-DB),[11] it seems possible that the H_2-passivation can deactivate some of the acceptor states from which the negative Q_{fix} originates. Apparently, a typically used Si/SiO_2 passivation process (400 °C, 1 h, 100% H_2) is (luckily) far less efficient for passivating the acceptor states than for P_b-type DB-defects at the Si/SiO_2 interface.[16] In addition to electrons from the Si-substrate, the P_b-type defects also represent a source of electrons to charge the acceptor states, as shown before by electron spin resonance (ESR).[12] Therefore, it is conceivable that their removal by H_2 results in less Q_{fix}.

The well-known efficiency of H_2-passivation in reducing interface traps (D_{it}) is shown in Fig. 1(b): D_{it} of the Al-free reference samples is reduced from $\sim 4 \times 10^{12}\ cm^{-2}\ eV^{-1}$ (orange data points) to $\sim 5 \times 10^{10}\ cm^{-2}\ eV^{-1}$ (black data points). Most surprisingly, the presence of only 6 Al–O MLs (~7.5 Å) separated by ≤2.5 nm tunnel-SiO_2 from the Si-surface, causes a D_{it} drop to the lower $10^{11}\ cm^{-2}\ eV^{-1}$ range (green data points, sample W), without any H_2-passivation. In fact, the additional passivation with H_2 (gray data points, sample W-H_2) decreases D_{it} only marginally in the tunnel-SiO_2 thickness range. For tunnel-SiO_2 thicknesses of ≥4 nm, D_{it} of sample W approaches the values of the Al-free reference. The extremely steep increase of D_{it} by one order of magnitude over less than 2 nm of tunnel-SiO_2 in sample W [green data points in Fig. 1(b)] does not resemble the tunnel-SiO_2 thickness function of the Q_{fix} density [red data points in Fig. 1(a)] and requires a detailed explanation. Please note that the D_{it} values reported in Fig. 1(b) refer to a Fermi energy at the Si/SiO_2 interface near the flatband condition, which for the substrate used here corresponds to ~0.88 eV above the Si valence band maximum.

The meanwhile established explanation for chemical passivation of thick ALD-Al_2O_3 films deposited directly on Si involves the passivation of DBs by hydrogen[17–19] and/or oxygen[20] diffusing from the Al_2O_3 to the Si/SiO_2 interface. This is supported by the fact that the typical annealing to activate the surface passivation is often at 400–450 °C for 15–30 min,[21] i.e., conditions well suited to H-passivate DBs at the Si/SiO_2 interface.[16] In contrast, the RTA conditions used here have a temperature far too high (900 °C) and a time far too short (30 s) for efficient interface defect passivation.[16] We note that the H-atoms available from just one ALD-Al_2O_3 cycle (even if assuming low H-concentrations of only ~1 at. %)[18] would be sufficient for an almost complete DB passivation. Also, the diffusion lengths of H- and O-related species from Al_2O_3 through the SiO_2 are several orders of magnitude longer during the RTA than the tunnel-SiO_2 thicknesses used here (for diffusion parameters, see, e.g., Ref. 22). Hence, chemical passivation of the Si-surface cannot be impeded by the critical ~4 nm tunnel-SiO_2 thickness found here, which clearly points toward an electronic explanation.

At the (100)Si/SiO_2 interface, two paramagnetic (singly occupied) and amphoteric defect centers are observed, P_{b0} and P_{b1}. The P_{b1} center is a Si point defect involving a strained Si-backbond,[23] whereas the P_{b0} center is configured as $Si_3{\equiv}Si\bullet$ (where • symbolizes the unpaired electron).[24] The P_{b0} center exhibits an electrically observable $0 \leftrightarrow 1$ charge transition level (sometimes also denoted +/0) at 0.3 eV above the Si valence band edge.[25] The electrical activity of P_{b1} as an interface trap is a matter of debate[26,27] but the reported $0 \leftrightarrow 1$ charge transition level is located ca. 0.45 eV above the Si valence band edge.[26]

In order to study the interaction of the interface defects with the Al-induced acceptor states in more detail, we plot in Fig. 2 their energy distribution over the bandgap for the samples with 1.2 nm tunnel-SiO_2. For the Al-free reference sample (orange data points), a clear peak at $E = E_V(Si) + 0.77$ eV is observed (dashed line), which corresponds to the $1 \leftrightarrow 2$ charge transition level of the P_{b0} center, i.e., the occupation of the singly occupied defect level with a second electron.[25] This peak is absent for all other samples, indicating that both H_2-passivation and Al–O MLs suppress the $1 \leftrightarrow 2$ charge transition of the P_{b0} center, in accordance with the data shown in Fig. 1(b). In the lower half of the bandgap, where the trap states cannot be probed with the high-frequency conductance method [Fig. 1(b)], the Al-free reference sample shows a high density of $0 \leftrightarrow 1$ charge transitions, which do not form a clear peak due to limitations of the analysis method (too high trap concentration and insufficient charge reversal of the defect states under strong inversion). However, both samples with Al–O MLs (green and gray data points) exhibit a distinct peak at $E = E_V(Si) + 0.28$ eV (dotted line) indicative of the $0 \leftrightarrow 1$ charge transition,[25] i.e., irrespective of H_2-passivation, whereas for the H_2-passivated reference sample, no peak in that energy range is observed.

The observation that the samples with Al–O MLs only allow for the $0 \leftrightarrow 1$ charge transition means that the defect level can still be occupied with one electron during the C-V measurements but not with a second electron, indicating that

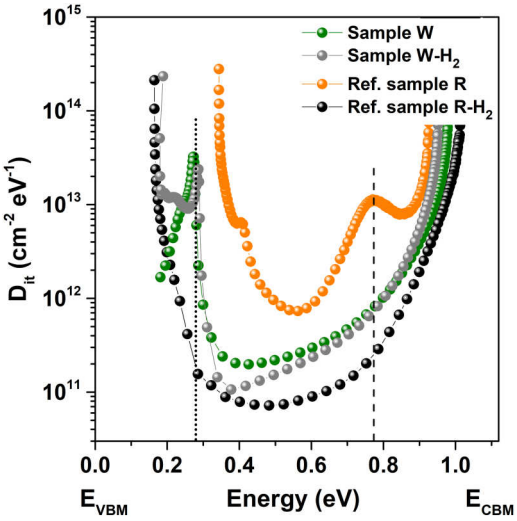

FIG. 2. Energy distribution of the interface defects over the bandgap for the samples with 1.2 nm tunnel-SiO_2. The $0 \leftrightarrow 1$ charge transition level is marked with a dotted line and the $1 \leftrightarrow 2$ charge transition level with a dashed line.

Published under license by AIP Publishing.

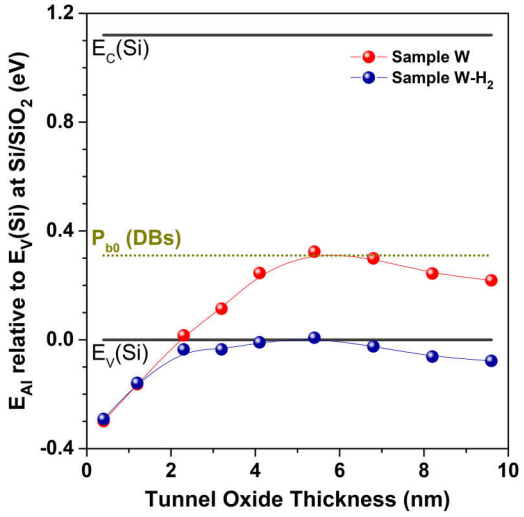

FIG. 3. Energy level of Al-induced acceptor states in SiO_2 (E_{Al}) as a function of tunnel-SiO_2 thickness relative to the valence band edge of Si at the interface to SiO_2 [E_V(Si)], calculated by a one-dimensional Poisson-Solver over the entire MIS structure. The P_{b0} defects originating from DBs at the Si/SiO_2 interface are located 0.3 eV above E_V(Si) as shown in dark yellow.

the defect is in the charge state 0 in its ground state. This strongly supports our explanation that Al-induced acceptor states in a tunneling distance to the Si/SiO_2 interface discharge the P_{b0} defect centers.

During annealing in H_2 gas, molecular hydrogen diffuses toward the Si/SiO_2 interface, dissociates at the Si DB and passivates the P_{b0} center via an Si–H bond.[16] Thereby, the unpaired electron of the Si-atom is fixed in a bond with H and no longer an electrically active point defect. Based on the electronegativity values (EN[H] = 2.2, EN[Si] = 1.7), H is anionic against Si so that the Si-atom has to provide the electron for the polar covalent Si–H bond. On first sight, it might appear as a surprise that the H_2-passivated Al–O sample (gray data points in Fig. 2) also shows the $0 \leftrightarrow 1$ charge transition (in contrast to the H_2-passivated reference sample, black data points). However, taking the above discussion and the process sequence into account, this can be explained as well: the Al-induced acceptor states are formed during RTA and immediately start capturing electrons from the P_{b0} centers, which discharges them and leaves no electron at the Si DB to bind to H during the subsequent H_2-annealing. Once discharged the P_{b0} centers cannot be chemically H_2-passivated anymore, but they can be temporarily occupied with an electron during the C-V measurement with a transition energy in the lower quarter of the Si-bandgap.

We calculate the energy level of the Al-induced acceptor E_{Al} relative to the Si valence band edge E_V(Si) at the Si/SiO_2 interface using a one-dimensional (1D) Poisson-Solver (coded in *MatLab* following Nicollian and Brews[15]) and the C-V data of Fig. 1. We presume for simplicity the ionized acceptor states to be at one depth position in the center of the 6 Al–O MLs instead of being located at both SiO_2/Al–O interfaces[12] (due to the ultrathin Al–O layer, the discrepancy is considered negligible) and having a relaxation energy of

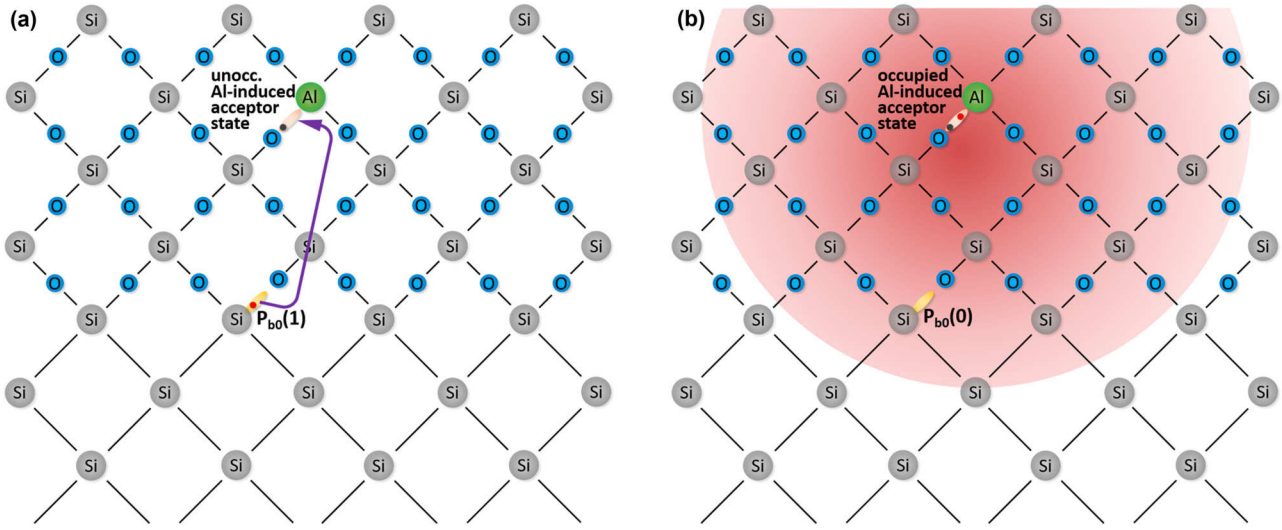

FIG. 4. Schematic illustration of the dangling bond discharge model. (a) In the initial state, the P_{b0} defect is occupied with one electron (charge state 1), whereas the Al-induced acceptor state at the Al–O/SiO_2 interface is unoccupied (Al^0). Tunneling of the electron from the P_{b0} defect into the acceptor state allows for a substantial energy relaxation. (b) After tunneling, the P_{b0} defect is unoccupied (charge state 0) and the acceptor state is occupied (Al^-). The additional electron in the dielectric has an electric field (indicated by the reddish sphere), which allows for field effect passivation. We note that the density of Al-acceptors in SiO_2 exceeds the interface trap density considerably.

Published under license by AIP Publishing.

$E_{Al} \approx E_V(Si) - 0.6$ eV.[11] Half of the 6 ML Al–O thickness was added to both the tunnel-SiO_2 and the capping-SiO_2. Figure 3 shows the E_{Al} values as a function of tunnel-SiO_2 thickness for the unpassivated and the H_2-passivated W-sample. With increasing tunnel-SiO_2 thickness, the high field strength of the charged acceptors induces a potential lift of their energy level. The strong drift field for ≤2.3 nm tunnel-SiO_2 leads to a nearly equal shift of E_{Al} against $E_V(Si)$ for both samples, which is corroborated by matching Q_{fix} values in Fig. 1(a). However, when E_{Al} raises above $E_V(Si)$, the samples show a very different behavior. For sample W-H_2, E_{Al} remains energetically very close to $E_V(Si)$ for all tunnel-SiO_2 thicknesses ≥2.3 nm. In contrast, the unpassivated sample W has a much steeper rise of E_{Al} over $E_V(Si)$ and reaches a maximum value of $E_V(Si) + 0.32$ eV for a tunnel-SiO_2 thickness of 5.4 nm. This energy coincides exactly with the $0 \leftrightarrow 1$ charge transition level of P_{b0} defects (indicated by the dark yellow dotted line in Fig. 3). Hence, no energy is gained by electrons tunneling from the P_{b0} defects into the Al-induced acceptor states, and consequently, the D_{it} values of sample W and the Al–O-free reference sample match for tunnel oxides ≥5.4 nm [cf. green and orange data points in Fig. 1(b)].

In other words, when considering the not-H_2-passivated sample, the P_{b0} defects are efficiently and nearly completely unoccupied (deactivated) due to the large energy difference for electron relaxation into Al-induced acceptor states for tunnel-SiO_2 thicknesses of up to ~3 nm. As E_{Al} approaches the charge transition level of the P_{b0} defects for tunnel oxides thicker than ~3 nm, the relaxation energy decreases and an increasing number of P_{b0} defects become reoccupied, which restores their recombination activity. Accordingly, D_{it} increases sharply around 3 nm tunnel-SiO_2 thickness [Fig. 1(b)].

We note that these results support the concept of the electrical inactivity of the P_{b1} defect as an interface trap, in accordance with Stesmans and Afanas'ev.[27]

An in-depth discussion of the tunneling properties, accompanying schematic band structures (Fig. 7) as well as a possible explanation for the E_{Al} decrease for tunnel oxides thicker than ~5 nm can be found in the Appendix.

The process of interface defect deactivation described so far implicates that a dangling bond defect electron becomes a fixed charge in the dielectric, i.e., the defect is not only deactivated, its electron is converted from a recombination center into the source of field-effect passivation as depicted schematically in Fig. 4. Hence, for sufficiently thin tunnel-SiO_2 thicknesses (≤3 nm), these combined electronic passivation mechanisms should result in excellent Si-surface passivation irrespective of chemical defect passivation by H_2.

Figure 5 shows MDP lifetime mappings at an injection level of ~10^{15} cm^{-3} of n-type Si half-wafers processed exactly in the same way as the electrically characterized samples discussed so far (except for symmetrical front- and back side SiO_2-wedge/Al–O MLs/SiO_2-stacks as usual for lifetime samples). Lifetimes of up to 1.4 ms are measured for sample W in the range of 2–3.5 nm tunnel-SiO_2, i.e., where Q_{fix} is high and D_{it} is small. This lifetime corresponds to an upper limit

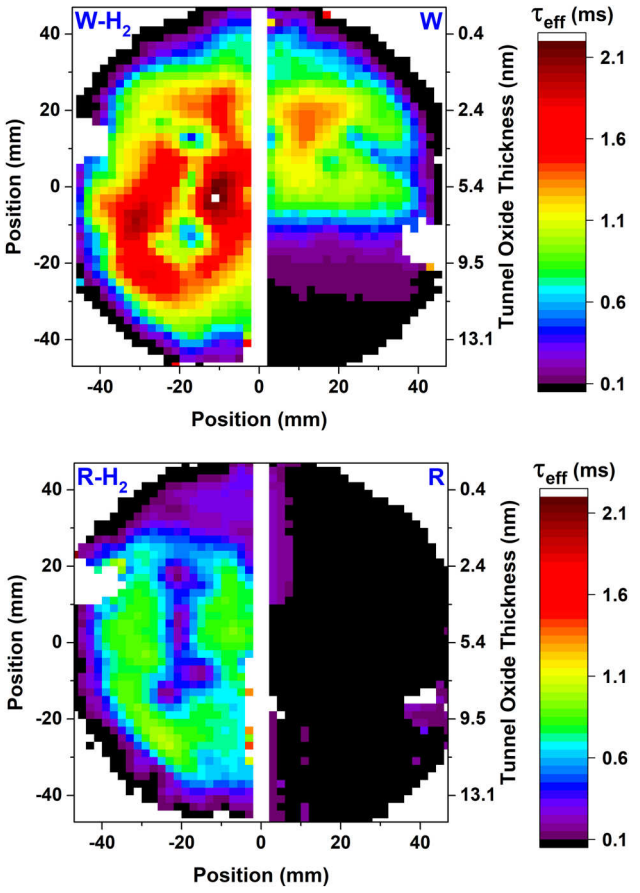

FIG. 5. Minority carrier lifetime (τ_{eff}) mappings at an injection level of ~10^{15} cm^{-3} of half-wafers with symmetrical SiO_2/Al–O-MLs/SiO_2-stacks with slant-etched, wedge-shaped tunnel-SiO_2 (W-samples) and Al–O-free references (R-samples), before and after H_2-passivation. The tunnel-SiO_2 thicknesses are plotted on the right *y* axes. For the W-samples, similar lifetimes beyond 1 ms are achieved in the optimum 2–3.5 nm tunnel-SiO_2 range, irrespective of H_2-passivation, while the R-H_2-sample shows less than half of that lifetime.

for the surface recombination velocity $S_{eff,max}$ of ~19 cm/s (using $S_{eff,max} = t_{wafer}/2\tau_{eff}$ with the bulk-lifetime $\tau_{bulk} \rightarrow \infty$ and t_{wafer} as the wafer thickness). The loss of high lifetimes toward thicker tunnel-SiO_2 is readily explained by a lower Q_{fix} density, causing less efficient field-effect passivation and the higher D_{it} densities. The reduced lifetimes for tunnel-SiO_2 thicknesses below 1 nm might be attributed to the vicinity of the wafer edge and associated lower surface quality. In addition, Si-surface contaminations from the nearly complete HF-etching of the oxide and subsequent handling can alter the interface properties. The mapping of sample W-H_2 demonstrates that H_2-passivation is not capable to significantly further improve the lifetimes in the optimum tunnel-SiO_2 thickness range (2–3.5 nm)—as presumed above. A major influence of H_2-passivation is mainly observed for tunnel-SiO_2

Published under license by AIP Publishing.

thicknesses above 4 nm, where the influence of the Al-induced acceptor states in D_{it} reduction is marginal. Still, sample W-H_2 has a significantly better surface passivation quality than the reference sample R-H_2, originating from the additional field effect passivation by a Q_{fix} of yet around -1×10^{12} cm^{-2} even for the thickest tunnel-SiO_2 used here [cf. Fig. 1(a)]. The unpassivated reference sample R has a featureless average lifetime of about 25 μs. Hence, the presence of just 6 Al–O MLs within a suitable tunnel distance from the substrate (sample W) therefore leads to a lifetime increase by a factor of more than 50.

A detailed discussion of the influence of H_2-passivation on the minority carrier lifetimes as a function of minority carrier density (photoconductance measurements) is provided in the supplementary material.

IV. CONCLUSIONS

In summary, we demonstrated that the midgap interface trap density (D_{it}) at the Si/SiO_2 interface can be reduced to a similar level as achieved by conventional H_2-passivation due to the presence of just a few Al–O MLs with Å-thicknesses on an ultrathin tunnel-SiO_2 of ≤2 nm thickness. The origin of this effect is the discharge of the P_{b0} DB-defects into Al-induced acceptor states in SiO_2. As a consequence, the discharged DB-defects are no longer deep recombination states so that Shockley-Read-Hall (SRH) recombination is drastically reduced. This constitutes an *interface defect deactivation* mechanism that is independent from field-effect passivation, i.e., the avoidance of surface recombination at neutral (singly occupied) DBs due to repelling one type of charge carrier by fixed charges in the dielectric. Nevertheless, the transfer of electrons from the P_{b0} defects into the Al-induced acceptor states generates a negative Q_{fix} that additionally enables field-effect passivation. The combination of this D_{it} reduction effect with field effect passivation results therefore in equal effective minority carrier lifetimes on n-type Si in the optimum tunnel-SiO_2 thickness range as chemical defect passivation by annealing in H_2. Furthermore, it was revealed that the discharged P_{b0} cannot be chemically passivated with H_2 due to the absence of an electron at the Si-DB to form the Si–H bond. Hence, a final annealing in H_2 (or forming gas) becomes a less important process step for the Si-surface passivation since most defects are already deactivated. Importantly, we find little evidence for a direct H_2-passivation of the Al-induced acceptor states.

The requirement for tunnel-SiO_2 thicknesses of below 3 nm to benefit from interface defect deactivation by the Al-induced acceptor states are in line with the parameters necessary to maximize Q_{fix}[12] and to enable efficient hole tunneling,[11] which represents optimum conditions for a passivating hole-selective contact for high-efficiency Si solar cells.

SUPPLEMENTARY MATERIAL

See supplementary material for photoconductance lifetime measurements of H_2-passivated and unpassivated samples.

ACKNOWLEDGMENTS

D.H. thanks the Alexander von Humboldt Foundation for a Feodor Lynen Fellowship and acknowledges funding by the German Research Foundation (DFG, HI 1779/3-1) and the Australian Centre for Advanced Photovoltaics (ACAP Collaboration Grant). D.H. and D.K. acknowledge funding by the DAAD–Universities Australia joint research cooperation scheme 2016 (No. 57215687). D.K. acknowledges the 2015 Blue Sky research grant of UNSW and the 2018 Theodore-von-Kármán-Fellowship of RWTH Aachen University.

APPENDIX: TUNNELING ENERGETICS AND DYNAMICS

In this appendix, we attempt to explain the energetics and dynamics of tunneling into the Al-induced acceptor states in SiO_2 leading to experimental results shown in Figs. 1 and 3.

Direct electron tunneling from the DBs into the Al-induced acceptor states is likely to become a time issue for tunnel-SiO_2 thicknesses (d_{t-Ox}) thicker than ~5 nm. A tremendous delay in electron relaxation into the acceptor states results from the macroscopic tunneling time constant $\tau_{T-macro}$. The time constant of the quantum-mechanical process τ_{T-QM}[28] (i.e., the inverse attempt frequency) is in the low fs range for an electron tunneling through a few nanometer of SiO_2. However, the *macroscopic time constant for exactly one electron being transferred through* SiO_2 is the product of τ_{T-QM} with the inverse of the electron tunneling probability T_T. While tunneling through ultra-thin barriers proceeds fast enough to extract even hot carriers prior to thermalization,[29] $\tau_{T-macro} = \tau_{T-QM}/T_T$ reaches months or even years for reasonably thick tunnel barriers. For instance, the near-completion of charging acceptor states by ionizing F-vacancies in AlF_3 layers on a comparatively thick (8.2 nm) tunnel-SiO_2 was observed after almost 4 years.[30] The same slow tunneling dynamics might influence the energetic position of Al-induced acceptors in SiO_2 relative to the valence band energy of Si [E_V(Si)] at the interface Si/SiO_2.

In Fig. 6, the energy level values of the Al-acceptor states (E_{Al}) relative to E_V(Si) as a function of tunnel-SiO_2 thickness as calculated by a one-dimensional Poisson-Solver are reproduced from Fig. 3. Figure 6 shows that the strong drift field of ca. 2.8 MV/cm (for $d_{t-Ox} = 0.4$ nm) to 1.6 MV/cm (for $d_{t-Ox} = 2.3$ nm) is nearly identical for both samples as evident from the nearly equal shift of E_{Al} against E_V(Si) with d_{t-Ox}, which is confirmed by the nearly identical Q_{fix} values in Fig. 1(a). For $d_{t-Ox} > 2.3$ nm, E_{Al} raises above E_V(Si) and the H_2-passivated and the unpassivated sample show significant differences.

For sample W-H_2, E_{Al} slowly increases with d_{t-Ox}, reaching a maximum of $E_{Al} = E_V(Si) + 0.007$ eV for $d_{t-Ox} = 5.4$ nm, before decreasing again to values just below E_V(Si). With electrons from E_V(Si) relaxing into Al modulation acceptors, their occupation probability P_{Al} is $P_{Al}(d_{t-Ox} = 5.4\text{ nm}) = \exp\{[E_{Al} - E_V(Si)]/k_BT\} = 0.43$ at $T = 300$ K. The maximum value of E_{Al} presents the equilibrium point at which E_{Al} stabilizes against E_V(Si) as indicated by the dashed blue line in Fig. 6. The decrease in E_{Al} for thicker d_{t-Ox} might be due to

Published under license by AIP Publishing.

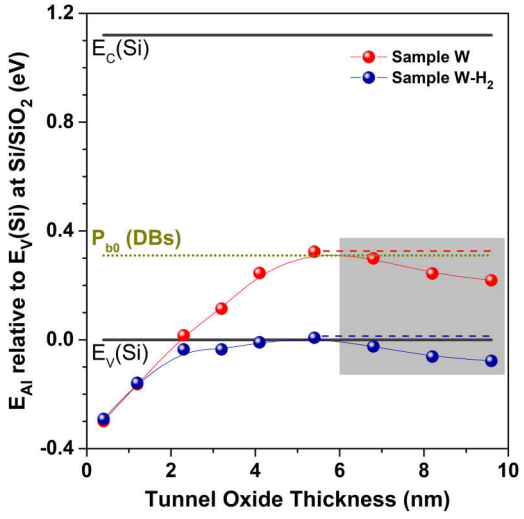

FIG. 6. Energy level of Al-induced acceptor states E_{Al} relative to the valence band edge of Si at the SiO_2-interface as a function of tunnel-SiO_2 thickness d_{t-Ox}. The calculated data as derived from a one-dimensional Poisson-Solver are the same as in Fig. 3. The decline of E_{Al} in the gray highlighted area might be due to increasingly reduced Al acceptor ionization by the large macroscopic tunneling time constant, which considerably delays the charge relaxation process. As proposed in the text, without this strong time dependence, E_{Al} should remain constant for $d_{t-Ox} > 5$ nm. This is indicated by the dashed lines. With increasing d_{t-Ox}, the drift field due to ionized Al-acceptors in SiO_2 decreases to keep the energy difference $E_{Al}(SiO_2) - E_V(Si)$ constant. As a result, the occupation probability P_{Al} of Al-acceptors decreases with increasing d_{t-Ox}, which leads to a decrease in Q_{fix} as shown in Fig. 1(a).

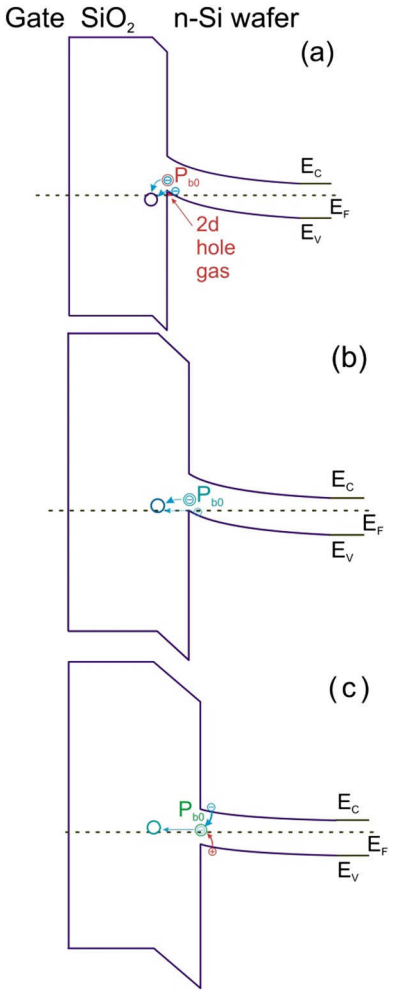

FIG. 7. Simplified band diagrams for the MIS structure of sample W with tunnel-SiO_2 thicknesses of 1 nm, 3 nm, and 5 nm based on the Q_{fix} and D_{it} data in Fig. 1 and the E_{Al} values in Fig. 3. (a) 1 nm tunnel-SiO_2: P_{b0} defects are efficiently discharged by Al-induced acceptor states due to a large energy difference between E_{Al} and $E_{P_{b0}}$ (relaxation energy). Furthermore, the acceptor states capture electrons from the Si valence band, which creates a two-dimensional hole gas in Si. (b) 3 nm tunnel-SiO_2: the E_{Al} level increases beyond E_V(Si) and ionization of Al-acceptor states with electrons from the Si valence band is energetically not favorable and no two-dimensional hole gas exists. In addition, the relaxation energy to the P_{b0} defects is significantly reduced so that some of the defects regain electrical activity as interface trap states D_{it} [cf. Fig. 1(b)]. (c) 5 nm tunnel-SiO_2: the relaxation energy for P_{b0} defect electrons vanishes as E_{Al} approaches $E_{P_{b0}}$. Therefore, the recombination at P_{b0} defects is widely restored and the D_{it} values of sample W equal those from the Al-acceptor-free reference sample.

the substantial time required to reach the charge equilibrium between the Si wafer and the Al-acceptor states. As mentioned, $\tau_{T-macro}$ increases exponentially with increasing tunnel barrier thickness d_{t-Ox} due to its inverse dependence on T_T.[30] This phenomenon is reflected in $E_{Al} \propto \mathrm{Max}(E_{Al}) \times \exp(-\tau_{T-macro}/t)$ and shown in Fig. 6 by the gray highlighted area. We note that t = constant since all samples were measured at the same (short) time after fabrication and the quotient in the exponent is in reverse to the usual arrangement due to $\tau_{T-macro} \propto 1/T_T$. Within this concept of the tunneling dynamics of electrons through SiO_2, the decrease of E_{Al} in the gray highlighted area in Fig. 6 would not be a direct feature of the Al-acceptors in SiO_2, but an effect related to the time delay in occupying the acceptor states through thick oxide barriers. Under this assumption, the dashed lines in Fig. 6 (blue for sample W-H_2, red for sample W) would be the evolution of E_{Al} with d_{t-Ox}.

Sample W has a much steeper rise of E_{Al} over E_V(Si) than sample W-H_2. Its maximum value of $E_{Al} = E_V(Si) + 0.324$ eV at the same d_{t-Ox} value of 5.4 nm as sample W-H_2 might be due to the same time conditions for electron tunneling. We will elucidate now what impact a H_2-passivation has on E_{Al} and P_{Al} as a function of d_{t-Ox}, whereby we focus on the d_{t-Ox} range not affected by tunneling dynamics. As shown by the reference sample in Fig. 1(b) (orange data points) traps states as represented by P_{b0} centers in the range of 4×10^{12} cm^{-2} are present at the Si/SiO_2 interface without H_2-passivation, which exceeds all Q_{fix} values of sample W measured by C-V [cf. Fig. 1(a)]. Such P_{b0} centers are occupied with one

Published under license by AIP Publishing.

electron and have a characteristic $0 \leftrightarrow 1$ charge transition energy of $E_{P_{b0}} = E_V(\mathrm{Si}) + 0.31$ eV at the interface Si/SiO_2.[25] These electrons have a preference for relaxing into Al acceptors over electrons relaxing from E_V(Si) since they lose more energy. This process is suppressed mainly by H_2-passivation of P_{b0} centers and—to a minor extent—by H_2-passivation of O-DBs at unoccupied Al acceptors which explains the much lower rise of E_{Al} over E_V(Si) with increasing d_{t-Ox}. The occupation probability of Al acceptors in sample W is $P_{Al}(d_{t-Ox} = 5.4\,\mathrm{nm}) = \exp[(E_{Al} - E_{P_{b0}})/k_BT] = 0.37$ at $T = 300$ K, which is very close to the $P_{Al}(d_{t-Ox} = 5.4\,\mathrm{nm})$ value of sample W-H_2. The conditions for Coulomb repulsion between ionized Al-acceptors in SiO_2 are virtually identical for both samples, resulting in ~1.4% of ionized acceptors.[12,31]

Figure 7 shows schematic band structures of sample W for d_{t-Ox} values of 1, 3, and 5 nm illustrating the discussion above. For ultra-thin tunnel-SiO_2 of 1 nm [Fig. 7(a)], electrons from P_{b0} defects relax into the Al-induced acceptor states in addition to electrons tunneling from the Si valence band into acceptor states, generating a two-dimensional hole gas in Si. As a consequence, P_{b0} defects cannot provide electrons for recombination with Si valence band holes, which deactivates their recombination activity. As d_{t-Ox} increases to 3 nm [Fig. 7(b)], the high field strength of charged Al acceptors induces a potential lift over the tunnel-SiO_2 which decreases their occupation probability, resulting in reduced Si band bending and the loss of hole-degeneracy. P_{b0} defects start to participate in surface recombination with the rising Fermi level (increasing occupation probability) due to reduced band bending in Si. Further increase in d_{t-Ox} to 5 nm [Fig. 7(c)] eventually leads to P_{b0} defects approaching their nominal occupation probability for undoped SiO_2 with the associated recombination activity.

REFERENCES

[1]H. Huang, J. Lv, Y. Bao, R. Xuan, S. Sun, S. Sneck, S. Li, C. Modanese, H. Savin, A. Wang, and J. Zhao, Sol. Energy Mater. Sol. Cells **161**, 14 (2017).
[2]D. K. Simon, P. M. Jordan, T. Mikolajick, and I. Dirnstorfer, ACS Appl. Mater. Interfaces **7**, 28215 (2015).
[3]C. Battaglia, A. Cuevas, and S. De Wolf, Energy Environ. Sci. **9**, 1552 (2016).
[4]B. Liao, B. Hoex, A. G. Aberle, D. Chi, and C. S. Bhatia, Appl. Phys. Lett. **104**, 253903 (2014).
[5]X. Yang, Q. Bi, H. Ali, K. Davis, W. V. Schoenfeld, and K. Weber, Adv. Mater. **28**, 5891 (2016).
[6]I. Dirnstorfer, T. Chohan, P. M. Jordan, M. Knaut, D. K. Simon, J. W. Bartha, and T. Mikolajick, IEEE J. Photovolt. **6**, 86 (2016).
[7]J. Bullock, M. Hettick, J. Geissbühler, A. J. Ong, T. Allen, C. M. Sutter-Fella, T. Chen, H. Ota, E. W. Schaler, S. De Wolf, C. Ballif, A. Cuevas, and A. Javey, Nat. Energy **1**, 15031 (2016).
[8]Y. Wan, C. Samundsett, J. Bullock, T. Allen, M. Hettick, D. Yan, P. Zheng, X. Zhang, J. Cui, J. McKeon, A. Javey, and A. Cuevas, ACS Appl. Mater. Interfaces **8**, 14671 (2016).
[9]C. Battaglia, S. Martín de Nicolás, S. De Wolf, X. Yin, M. Zheng, C. Ballif, and A. Javey, Appl. Phys. Lett. **104**, 113902 (2014).
[10]M. Bivour, J. Temmler, H. Steinkemper, and M. Hermle, Sol. Energy Mater. Sol. Cells **142**, 34 (2015).
[11]D. König, D. Hiller, S. Gutsch, M. Zacharias, and S. Smith, Sci. Rep. **7**, 46703 (2017).
[12]D. Hiller, J. Göttlicher, R. Steininger, T. Huthwelker, J. Julin, F. Munnik, M. Wahl, W. Bock, B. Schoenaers, A. Stesmans, and D. König, ACS Appl. Mater. Interfaces **10**, 30495 (2018).
[13]J. R. Brews, Solid State Electron. **26**, 711 (1983).
[14]M. Kuhn, Solid State Electron. **13**, 873 (1970).
[15]E. H. Nicollian and J. R. Brews, *MOS Physics and Technology* (Wiley & Sons, New York, 1982).
[16]A. Stesmans, J. Appl. Phys. **88**, 489 (2000).
[17]M. Schnabel, B. W. H. van de Loo, W. Nemeth, B. Macco, P. Stradins, W. M. M. Kessels, and D. L. Young, Appl. Phys. Lett. **112**, 203901 (2018).
[18]G. Dingemans, F. Einsele, W. Beyer, M. C. M. van de Sanden, and W. M. M. Kessels, J. Appl. Phys. **111**, 093713 (2012).
[19]A. Richter, J. Benick, M. Hermle, and S. W. Glunz, Appl. Phys. Lett. **104**, 061606 (2014).
[20]R. Chaukulkar, W. Nemeth, A. Dameron, P. Stradins, and S. Agarwal, in *IEEE Photovoltaic Specialist Conference* (IEEE, 2014).
[21]B. Hoex, J. J. H. Gielis, M. C. M. van de Sanden, and W. M. M. Kessels, J. Appl. Phys. **104**, 113703 (2008).
[22]S. W. Jones, *Diffusion in Silicon* (IC Knowledge LCC, Georgetown, MA, 2008), pp. 34–35.
[23]A. Stesmans, B. Nouwen, and V. V. Afanas'ev, Phys. Rev. B **58**, 15801 (1998).
[24]C. R. Helms and E. H. Poindexter, Rep. Prog. Phys. **57**, 791 (1994).
[25]E. H. Poindexter, G. J. Gerardi, M.-E. Rueckel, P. J. Caplan, N. M. Johnson, and D. K. Biegelsen, J. Appl. Phys. **56**, 2844 (1984).
[26]G. J. Gerardi, E. H. Poindexter, P. J. Caplan, and N. M. Johnson, Appl. Phys. Lett. **49**, 348 (1986).
[27]A. Stesmans and V. V. Afanas'ev, J. Phys. Condens. Matter **10**, L19 (1998).
[28]C. Bracher, M. Kleber, and M. Riza, Phys. Rev. B **60**, 1864 (1999).
[29]D. König, D. Hiller, M. Zacharias, S. Michard, and C. Flynn, Progr. Photovolt. **22**, 1070 (2014).
[30]D. König, M. Rennau, and M. Henker, Solid State Electron. **51**, 650 (2007).
[31]D. König, D. Hiller, and S. Smith, Phys. Rev. Appl. **10**, 054034 (2018).

Published under license by AIP Publishing.